JACS
JOURNAL OF THE AMERICAN CHEMICAL SOCIETY

pubs.acs.org/JACS

Article

Zn-Promoted C−H Reductive Elimination and H_2 Activation via a Dual Unsaturated Heterobimetallic Ru−Zn Intermediate

Fedor M. Miloserdov,* Nasir A. Rajabi, John P. Lowe, Mary F. Mahon, Stuart A. Macgregor,* and Michael K. Whittlesey*

Cite This: J. Am. Chem. Soc. 2020, 142, 6340−6349

Read Online

ACCESS | Metrics & More | Article Recommendations | Supporting Information

ABSTRACT: Reaction of $[Ru(PPh_3)_3HCl]$ with $LiCH_2TMS$, $MgMe_2$, and $ZnMe_2$ proceeds with chloride abstraction and alkane elimination to form the bis-cyclometalated derivatives $[Ru(PPh_3)(C_6H_4PPh_2)_2H][M']$ where $[M']$ = $[Li(THF)_2]^+$ (**1**), $[MgMe(THF)_2]^+$ (**3**), and $[ZnMe]^+$ (**4**), respectively. In the presence of 12-crown-4, the reaction with $LiCH_2TMS$ yields $[Ru(PPh_3)(C_6H_4PPh_2)_2H][Li(12\text{-crown-}4)_2]$ (**2**). These four complexes demonstrate increasing interaction between M′ and the hydride ligand in the $[Ru(PPh_3)(C_6H_4PPh_2)_2H]^-$ anion following the trend **2** (no interaction) < **1** < **3** < **4** both in the solid-state and solution. Zn species **4** is present as three isomers in solution including square-pyramidal $[Ru(PPh_3)_2(C_6H_4PPh_2)(ZnMe)]$ (**5**), that is formed via C−H reductive elimination and features unsaturated Ru and Zn centers and an axial Z-type $[ZnMe]^+$ ligand. A $[ZnMe]^+$ adduct of **5**, $[Ru(PPh_3)_2(C_6H_4PPh_2)(ZnMe)_2][BAr^F{}_4]$ (**6**) can be trapped and structurally characterized. **4** reacts with H_2 at −40 °C to form $[Ru(PPh_3)_3(H)_3(ZnMe)]$, **8-Zn**, and contrasts the analogous reactions of **1**, **2**, and **3** that all require heating to 60 °C. This marked difference in reactivity reflects the ability of Zn to promote a rate-limiting C−H reductive elimination step, and calculations attribute this to a significant stabilization of **5** via Ru → Zn donation. **4** therefore acts as a latent source of **5** and this operational "dual unsaturation" highlights the ability of Zn to promote reductive elimination in these heterobimetallic systems. Calculations also highlight the ability of the heterobimetallic systems to stabilize developing protic character of the transferring hydrogen in the rate-limiting C−H reductive elimination transition states.

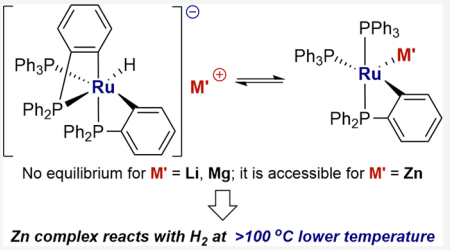

INTRODUCTION

Oxidative addition and reductive elimination are fundamental steps in the transition metal (TM)-mediated activation and transformation of organic molecules under both stoichiometric and catalytic conditions.[1] Efforts to enhance these processes at a TM center typically focus on modifying the steric and electronic properties of the surrounding ligands, which usually feature nonmetallic elements (P, N, O, C, Hal, etc.). In contrast, the use of main group metals (M′) as ligands for TMs has received far less attention.[2−8] However, there are isolated examples showing that the presence of a TM−M′ interaction can bring about transformative changes to the reactivity of the TM center. For example, Bergman and Tilley have shown that whereas neither $[(phen)PtAr_2]$ nor $[(bipy)PtAr_2]$ (Ar = p-^{t}BuC_6H_4) undergo reductive elimination of biaryl even after 48 h at 200 °C, the reaction is complete within just 15 min at 60 °C upon addition of 10 equiv $Zn(C_6F_5)_2$.[9] The possibility of tuning a TM center toward reductive elimination (or possibly the reverse, oxidative addition) by judicious choice of M′ is intriguing and indeed has been demonstrated with Ni−M′ heterobimetallics (**I**, Scheme 1) where a polydentate ligand scaffold supports the Ni−M′ interaction. The Ni−Ga species was found to perform best for both alkene[10] and CO_2 hydrogenation;[11] however, in addition to promoting oxidative addition, it has been conjectured that M′ may also enhance reactivity by facilitating the ligand dissociation that is necessary in these systems or by stabilizing hydride intermediates.[12] Defining the role of M′ in these and other related metalloligand scaffolded systems such as **II**,[13] **III**,[14] and **IV**[15] is therefore a challenge.

We have recently reported the preparation of a series of heterobimetallic Ru−M′ (M′ = Zn, Ga, and In) complexes by reaction of the cationic N-heterocyclic carbene (NHC) ruthenium hydride precursor $[Ru(IPr)_2(CO)H]^+$ with M′−alkyls (M′ = Zn, Ga, In).[16−18] The reactions proceed through simple elimination of an alkane[19−28] to afford products featuring unsupported and unconstrained Ru−M′ bonds, **V** and **VI**, in which (in contrast to metalloligand scaffold systems) both the TM and M′ centers are coordinatively unsaturated (Scheme 1). This "dual unsaturation" allows these Ru−M′ complexes to react with both E−H bonds (E = H, B, and Si) and CO; moreover, these systems proved amenable to detailed mechanistic studies that delineate the role of the Ru−

Received: January 28, 2020
Published: March 5, 2020

https://dx.doi.org/10.1021/jacs.0c01062
J. Am. Chem. Soc. 2020, 142, 6340−6349

Scheme 1. TM-M′ Heterobimetallic Complexes[16]

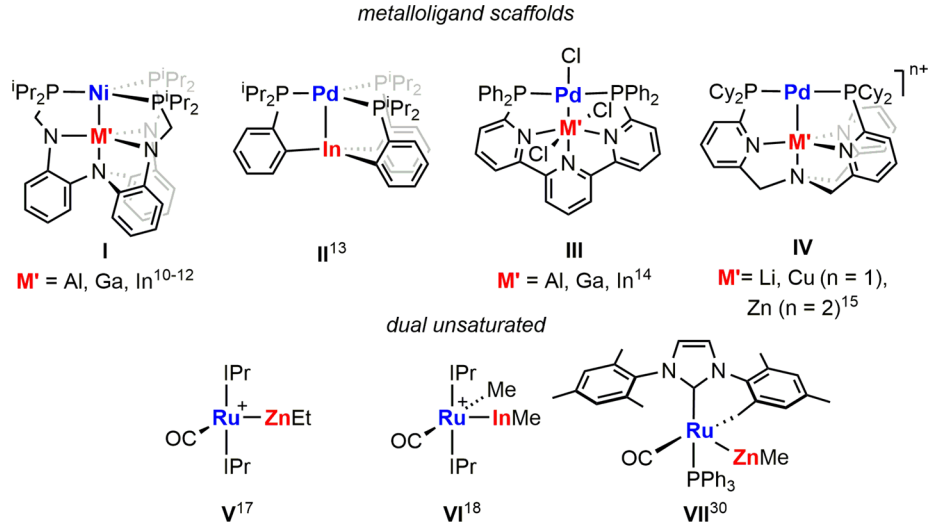

Scheme 2. Synthetic Routes to 1−4

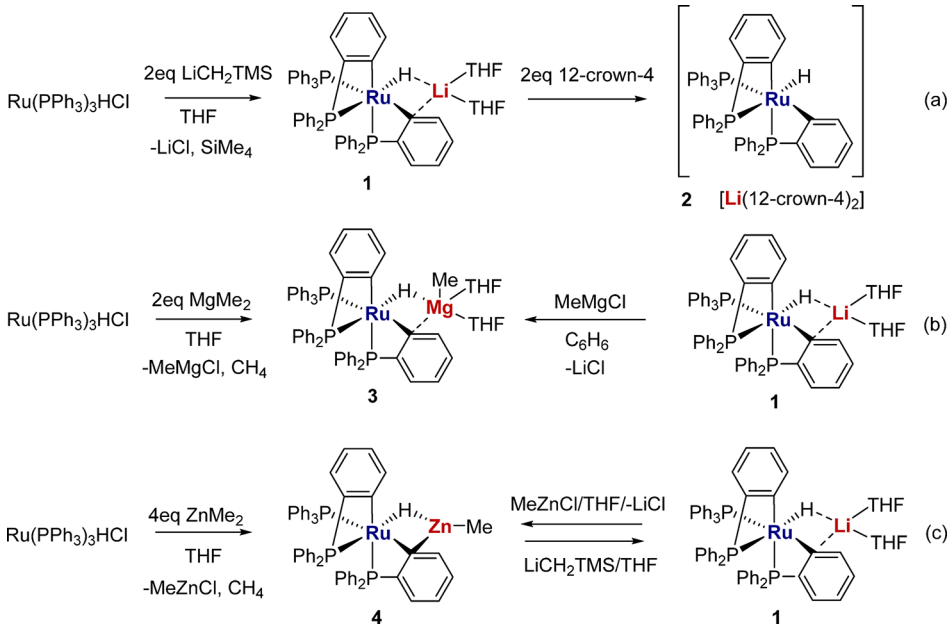

M′ moiety in promoting these processes. Subsequently, alkane loss was also observed upon addition of $ZnMe_2$ to the neutral precursor $[Ru(IMes)(PPh_3)(CO)HCl]$,[29] showing that an electrophilic TM−H precursor is not a prerequisite for alkane elimination to take place.[30] Two equivalents of CH_4, along with MeZnCl, are now lost, with the second 'H' arising from cyclometalation of the IMes ligand to give **VII** (Scheme 1). This cyclometalation strategy was then exploited to form further Ru−Zn heterobimetallics through the reaction of $ZnMe_2$ and $[Ru(PPh_3)_3Cl_2]$, showing that alkane loss can be induced even from simple, nonhydride-containing TM precursors.[31]

In light of this reactivity, our attention was drawn to the report by Cole-Hamilton and Wilkinson in 1977 on the reactions of $[Ru(PPh_3)_3HCl]$ with Zn, as well as Li and Mg, alkyls.[32] These were reported to yield heterobimetallic products containing the cyclometalated $\{RuH(C_6H_4PPh_2)(PPh_3)_2\}$ fragment, albeit with structures that were poorly defined. Following a reinvestigation of these reactions, we now show that the products are in fact $[Li(THF)_2]^+$ (**1**), $[MgMe(THF)_2]^+$ (**3**), and $[ZnMe]^+$ (**4**) derivatives of the bis-cyclometalated anion, $[Ru(PPh_3)(C_6H_4PPh_2)_2H]^-$, which originate upon elimination of two equivalents of CH_4, along with M′Cl and cyclometalation of the PPh_3 ligand. These species, together with a $[Li(12\text{-crown-}4)_2]^+$ derivative (**2**), have allowed us to undertake a comparative study of the influence of M′ on the reactivity of a common Ru fragment. A combination of experiment and computation has revealed a remarkable acceleration of C−H bond reductive elimination when M′ = ZnMe, resulting in the formation of an equilibrium mixture of the complex $[Ru(PPh_3)(C_6H_4PPh_2)_2H(ZnMe)]$ (**4**) and its dual unsaturated isomer $[Ru(PPh_3)_2(C_6H_4PPh_2)(ZnMe)]$ (**5**). As a result of this operational dual unsaturation, **4** reacts with H_2 at −40 °C, whereas the Li and Mg derivatives require heating at 60 °C to demonstrate equivalent reactivity, a difference of 100 °C.

https://dx.doi.org/10.1021/jacs.0c01062
J. Am. Chem. Soc. 2020, 142, 6340−6349

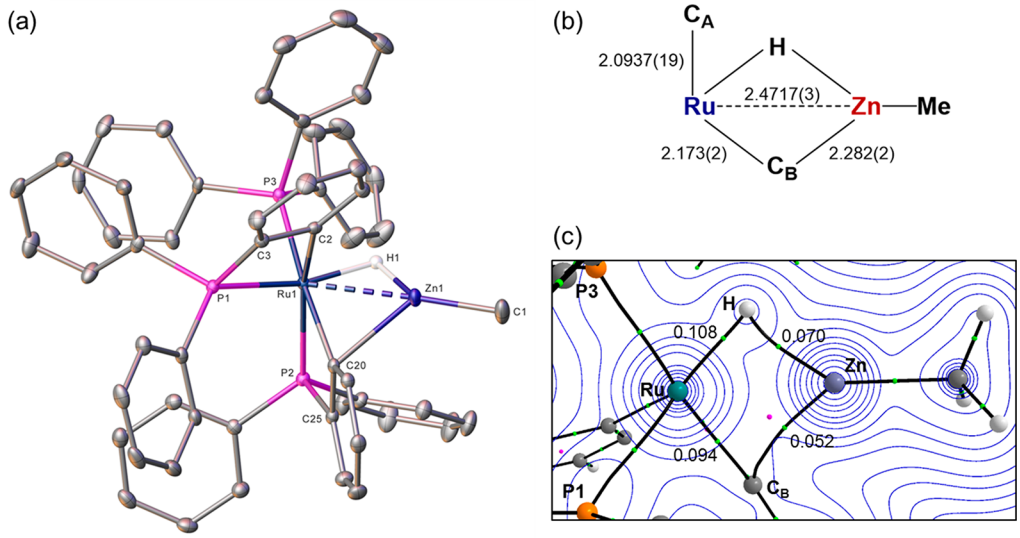

Figure 1. (a) Molecular structure of **4**. Ellipsoids are represented at 30% probability. Only the major component of the disordered phenyl group ligand (attached to P3) is shown. Hydrogen atoms, with the exception of H1, have also been omitted for clarity. (b) Summary of key distances in **4**. (c) Detail of the QTAIM molecular graph for **4** showing key bond critical points (BCPs, green spheres) and ring critical points (RCPs, pink spheres) with associated BCP electron densities, $\rho(r)$, in a.u. The experimental structure was employed with the H atoms optimized, giving Ru1−H1 and Zn1−H1 distances of 1.69 and 1.80 Å, respectively (Supporting Information).

Table 1. Comparison of Key Structural, NMR (THF-d_8), and QTAIM Parameters (in a.u.) for 1−4

parameter		2	1	3	4
M′		$Li(crown)_2$	$Li(THF)_2$	$MgMe(THF)_2$	ZnMe
Ru···M′ (Å)		–	2.825(6)	2.8250(8)	2.4717(3)
M′···C_B (Å)		–	2.317(7)	2.596(2)	2.282(2)
$^2J_{RuH-PA}$ (Hz)		93.3	83.9	68.0	51.3
			QTAIM data		
Ru−H BCP	$\rho(r)$	0.130	0.114	0.112	0.108
	ε	0.008	0.011	0.051	0.065
	H(r)	−0.061	−0.047	−0.044	−0.043
M′···H BCP	$\rho(r)$	–	0.019	0.029	0.070
	ε	–	0.421	0.478	0.337
	H(r)	–	0.003	0.001	−0.019
Zn−C_B BCP	$\rho(r)$				0.052
	ε				0.021
	H(r)				−0.010

RESULTS AND DISCUSSION

Synthesis and Characterization of $[Ru(PPh_3)(C_6H_4PPh_2)_2H][M']$ Complexes (M′ = $Li(THF)_2$ (1), $[Li(12\text{-crown-}4)_2]$ (2), $MgMe(THF)_2$ (3), and ZnMe (4)). $[Ru(PPh_3)_3HCl]$ reacts instantaneously with 2 equiv $LiCH_2TMS$ in THF to eliminate LiCl and $SiMe_4$ and form $[Ru(PPh_3)(C_6H_4PPh_2)_2H][Li(THF)_2]$ (**1**, Scheme 2a), rather than $[Ru(PPh_3)_2(THF)(C_6H_4PPh_2)H]$ as previously proposed.[32] The presence of two cyclometalated phosphines[33−36] was apparent from the appearance of two low-frequency $^{31}P\{^1H\}$ NMR resonances at δ −20.7 and δ −25.1.[36,37] Together with the presence of a single high frequency ^{31}P signal (δ 53.3) and $^2J_{PP}$ values of 17−22 Hz, these data are consistent with the three phosphorus centers adopting a fac geometry (Scheme 2). The ^1H NMR and X-ray data for **1** show evidence for a close association of the $[Li(THF)_2]^+$ moiety with the $[Ru(PPh_3)(C_6H_4PPh_2)_2H]^-$ anion and are discussed in detail below. Complete separation of the lithium ion in **1** was induced upon addition of 12-crown-4[38] in benzene, to yield $[Ru(PPh_3)(C_6H_4PPh_2)_2H]^-$ with a $[Li(12\text{-crown-}4)_2]$ cation (**2**, Scheme 2a) in 74% isolated yield (ESI).

The analogous reaction of $[Ru(PPh_3)_3HCl]$ with $MgMe_2$ in THF afforded a Mg-containing analogue of **1**, fac-$[Ru(PPh_3)(C_6H_4PPh_2)_2H][MgMe(THF)_2]$ (**3**, Scheme 2b). Unlike **1**, the synthesis of **3** was less selective (ca. 85% yield of **3** based on NMR) and also presented difficulties in separating the product from the MeMgCl byproduct. **3** was therefore best prepared via Li/Mg metathesis of **1** with MeMgCl. Similarly the reaction of $[Ru(PPh_3)_3HCl]$ with $ZnMe_2$ gave the related Zn complex, $[Ru(PPh_3)(C_6H_4PPh_2)_2H(ZnMe)]$ (**4**, Scheme 2c). The formation of M′−Cl-containing byproducts once more proved problematic (ESI), and the synthesis of byproduct-free **4** was achieved through exchange of **1** with MeZnCl (generated *in situ* upon reaction of $[Ru(PPh_3)_3HCl]$ with $ZnMe_2$; ESI). In contrast to the strong coordination of THF to Li and Mg in **1** and **3**, THF readily dissociated from Zn in **4** (ESI)[39] and complexes with and without coordinated THF could be isolated, depending on crystallization conditions (Supporting Information). As shown in Scheme 2c, Zn/Li

https://dx.doi.org/10.1021/jacs.0c01062
J. Am. Chem. Soc. 2020, 142, 6340−6349

exchange was also possible, affording **1** cleanly and in good yield upon addition of $LiCH_2TMS$ to **4** in THF.

Experimental and Computational Analysis of 1−4. The level of interaction between the hydridoruthenate $[Ru(PPh_3)(C_6H_4PPh_2)_2H]^-$ and the different [M′] cations in **1**−**4** (M′ = $Li(THF)_2$, Li(12-crown-4)$_2$, $MgMe(THF)_2$, and ZnMe, respectively) was analyzed using a combination of single crystal X-ray diffraction (Figure 1; Tables 1 and S7), multinuclear NMR spectroscopy (Tables 1 and S6), and DFT calculations (Figure 1, Table 1). Across all four compounds, $[Ru(PPh_3)(C_6H_4PPh_2)_2H]^-$ exhibited the same distorted octahedral[40−43] structure, with a fac-arrangement of the three phosphine ligands and the hydride trans to the P atom of one of the cyclometalated $C_6H_4PPh_2$ groups. For **1** and **2**, the Ru···$Li(THF)_2$ and Ru···$MgMe(THF)_2$ distances were identical [2.825(6) and 2.8250(8) Å, respectively]. The Ru···Li value was longer than the sum of the two covalent radii (2.74 Å), whereas with Mg, it was slightly shorter (2.87 Å).[44] In the case of **4** (M′ = ZnMe), the Ru···Zn distance (2.4717(3) Å) was now much reduced (Σcovalent radii = 2.68 Å).[44] **4** also displayed a rather short Zn−C_B (Table 1, Figure 1b) distance of 2.282(2) Å [comparable to the π-interactions in $[ZnPh_2]_2$ (2.364(5)-2.442(4) Å)][45] and, as a result, an elongated Ru−C_B distance [2.173(2) Å; cf. Ru−C_A 2.0937(19) Å].

The degree of interaction between the Ru−hydride and M′ was also reflected in the magnitude of the trans H−Ru−P coupling constant. Thus, **2**, which is a separated ion-pair and therefore features a terminal Ru hydride ligand, displayed a trans $^2J_{HP}$ splitting of 93 Hz.[46] The stronger Ru−H···ZnMe interaction in complex **4** reduces this value to 51 Hz. **1** and **3** showed intermediate coupling constants, leading to an overall order of trans $^2J_{HP}$ of **2** > **1** > **3** > **4** (Table 1).[47] This order correlates well with the changes in hydride character seen in a Quantum Theory of Atoms in Molecules (QTAIM) study of these systems (Figure 1c, Table 1). Thus, the electron density, $\rho(r)$, associated with the Ru−H bond critical point (BCP) reduces from 0.130 au in **2** to 0.114 au and 0.112 au in **1** and **3** and then to 0.108 in **4**. This suggests a weakening of the Ru−H covalent interaction that is also reflected in the reduced (negative) values of the total energy density, H(r), along this series. The Ru−H BCP ellipticities (ε) also indicate increasing bridging character from **1** to **3** and **4** and compare with **2** where the near-zero value is consistent with a terminal Ru−H σ-bond.[48] Accordingly Li−H, Mg−H, and Zn−H bond paths are all identified for **1**, **3**, and **4** with increasing $\rho(r)$ values. Although the associated total energy densities, H(r), are always small, they do move from positive to negative values along this series, suggesting a trend toward increased covalency. A Zn−C_B bond path is also seen for **4**, as well as a ring critical point (RCP) associated with the {Ru−H−Zn−C_B} unit. No equivalent M′−C_B bond path is seen for either **1** or **3**. The lack of a Ru···M′ bond path in all of these species suggests no direct Ru−M′ interaction despite, in the case of **4**, the Ru−Zn distance being well within the sum of the covalent radii. Bonding character is therefore diverted through the bridging hydride and C_B positions.[49]

Solution Behavior of 4. Upon dissolution, yellow crystals of **4** afforded red solutions,[32] which by NMR spectroscopy, revealed the fac configuration of the complex to be the major component, along with two minor species, assigned as further isomers (Scheme 3; for clarity, fac- and mer-**4** will be used when discussing solution behavior, whereas **4** will be used for solid-state phenomena). The ratio of the three isomers was

Scheme 3. Isomers of 4 Observed in Solution

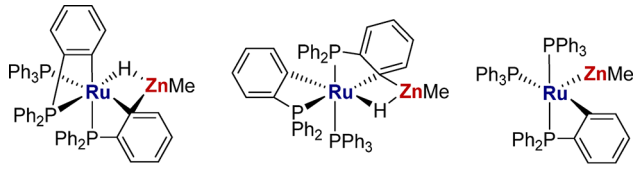

somewhat solvent-dependent (50:2:1 in THF-d_8 and 75:3:2 in C_6D_6) but was invariant both with time (weeks at room temperature) and between different batches of **4**.

The more prominent of the minor components (ca. 4% intensity) was assigned as mer-**4** based on the presence of three ^{31}P NMR signals (δ −20.4, −25.3, and 54.8, with $^2J_{PP}$ values of 25 and 272 Hz) and a hydride resonance with cis couplings to all three phosphorus centers ($^2J_{HP}$ = 16, 11, and 5 Hz). As a result of their coordinative saturation, fac- and mer-**4** would be expected to generate colorless or yellow solutions, implying that the red coloration of the reaction mixture results from the second of the minor isomers (ca. 2% intensity). This species, **5**, was therefore assigned as the coordinatively dual unsaturated complex, $[Ru(PPh_3)_2(C_6H_4PPh_2)ZnMe]$, which contains a direct Ru−Zn bond (Scheme 3). The assignment was substantiated by the $^{31}P\{^1H\}$ NMR data, which indicated a mer-arrangement of phosphine ligands in **5**, of which only one was now cyclometalated. There was no evidence for Li or Mg analogues of **5** by NMR spectroscopy in solutions of **1** or **3**.

Additional support for the identity of **5** was provided by the isolation and structural characterization of the cationic $[ZnMe]^+$-trapped derivative, $[Ru(PPh_3)_2(C_6H_4PPh_2)(ZnMe)_2][BAr^F{}_4]$ (**6**),[50] formed upon reaction of **4** with $MeZnCl/NaBAr^F{}_4$ (Figure 2). Although **6** was stable in benzene, toluene, and fluorobenzene, it eliminated $[ZnMe]^+$ and underwent metalation of one of the two PPh_3 ligands in THF, reforming a mixture of fac- and mer-**4** and **5**. Figure 2 outlines a proposed pathway to **6**, which involves chloride abstraction from MeZnCl (generated alongside **4** in the initial reaction of $[Ru(PPh_3)_3HCl]$ and $ZnMe_2$) by $NaBAr^F{}_4$, followed by reaction of the resulting $[ZnMe]^+$ with **5**.

Formation of 5 through Zn-Facilitated Reductive Elimination at 4. The formation of **5** arises upon reductive elimination from fac-**4**. This could involve either of the two cyclometalated aryl rings (i.e., carbons C_A or C_B, Figure 3) cis to Ru−H. The complete assignment of the phosphorus signals in both fac-**4** and **5**, together with $^{31}P\{^1H\}$ EXSY measurements, revealed that only the aryl group bridging the Ru and Zn centers (leading to C_B−H bond formation, Figure 3) was involved.[51] The absence of cross-peaks between mer-**4** and either fac-**4** or **5** suggested that the metalation of **5** to give the mer-isomer of **4** has a higher barrier than that for the fac-isomer (vide infra).

The various reductive elimination pathways were explored with density functional theory (DFT) calculations. Geometries and associated thermodynamic corrections were computed with the BP86 functional, with electronic energies recomputed with ωB97x-D and including corrections for toluene solvent and a larger def2-TZVP basis set. This protocol best captured the relative free energies of the various species implied from the solution NMR speciation studies. Thus, ***fac*-4** (0.0 kcal/mol) was computed to be most stable and is the dominant species in solution over ***mer*-4** (+1.8 kcal/mol) and **5** (+3.7

https://dx.doi.org/10.1021/jacs.0c01062
J. Am. Chem. Soc. 2020, 142, 6340−6349

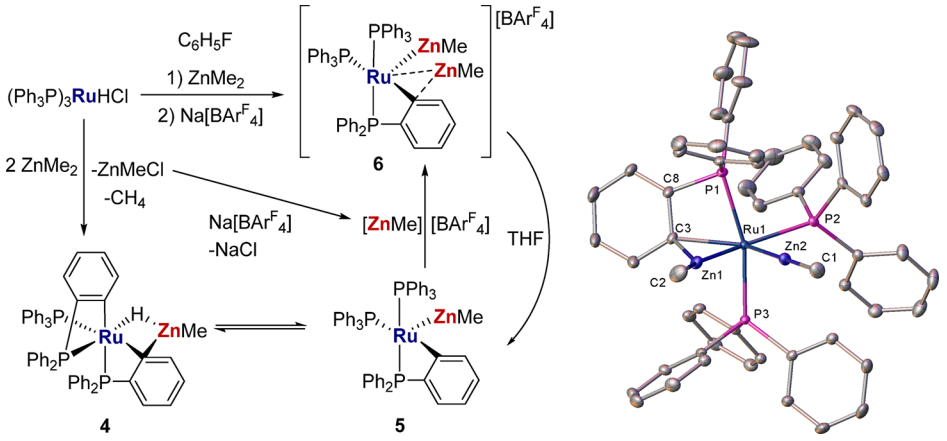

Figure 2. Pathway to formation of **6** (left) and X-ray structure of the cation in **6** (right). Ellipsoids are represented at 30% probability, and all hydrogens have been omitted for clarity. Selected bond lengths (Å) and angles (deg): Ru(1)−Zn(1) 2.5503(4), Ru(1)−Zn(2) 2.4107(3), Ru(1)−C(3) 2.194(3), Zn(1)−Zn(2) 2.6754(4), and Zn(1)−Ru(1)−Zn(2) 65.198(12).

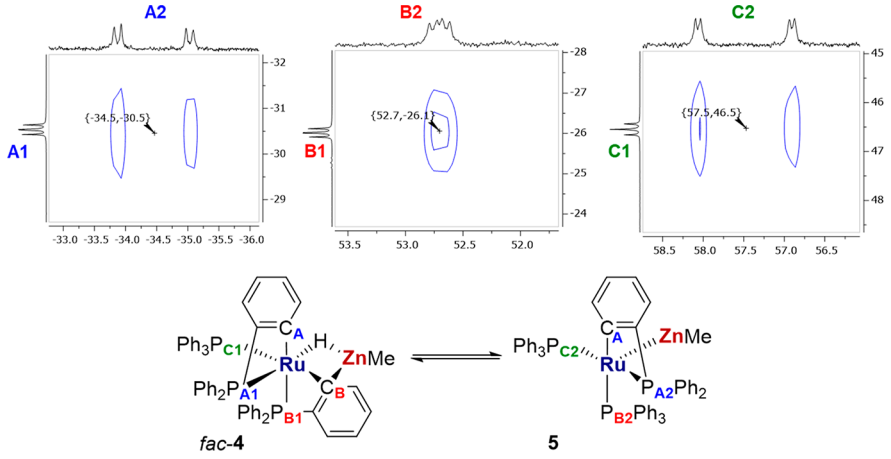

Figure 3. $^{31}P\{^{1}H\}$ EXSY illustrating the equilibrium between fac-**4** and **5**.

kcal/mol). Geometries were obtained after extensive conformational searching following our published protocol (see the Supporting Information for full details and functional testing).[52]

Figure 4 shows C_B−H reductive elimination in ***fac*-4** to form **5** proceeds in two steps involving first rotation about the Ru···Zn vector via **TS1**$(fac\text{-}4\text{−}5)_B$ followed by C_B−H bond formation via **TS2**$(fac\text{-}4\text{−}5)_B$. This second step is coupled to an isomerization that moves P_A cis to the new ZnMe moiety that is itself trans to the vacant site. C−H bond coupling is accompanied by some shortening of the Ru−Zn distance in **TS2**$(fac\text{-}4\text{−}5)_B$ (2.47 Å) which is then even more pronounced in **5** (2.37 Å) in which both the Ru and Zn centers are unsaturated. The overall barrier for the formation of **5** from ***fac*-4** is +18.5 kcal/mol. In ***fac*-4**, C_A is already cis to the hydride and so C_A−H reductive elimination can proceed directly through **TS**$(fac\text{-}4\text{−}5)_A$ to form **Int**$(fac\text{-}4\text{−}5)_A$, an isomer of **5** with an agostic interaction trans to P_B. This process has a higher barrier of +20.9 kcal/mol, possibly as the Ru−H bond is initially coplanar with the cyclometalated C_A ring and some distortion is required to access the transition state geometry. In contrast, the Ru−H bond in **Int**$(fac\text{-}4\text{−}5)_B$ is perpendicular to the C_B ring which facilitates the coupling process. Reductive elimination in ***mer*-4** was also computed and entails a transition state at +21.8 kcal/mol (ESI). Thus, C_B−H reductive elimination in ***fac*-4** is the easiest of these three processes, consistent with it being the dominant process observed experimentally. The square-pyramidal structure of **5** with an axial ZnMe ligand reflects the high trans influence of the $[ZnMe]^+$ moiety,[53] and a more detailed electronic structure analysis of this species is presented below.

Reaction of Complexes 1−4 with H_2. Complexes **1**−**3** reacted with H_2 (1 atm, THF-d_8) only at 60 °C, leading to 50% depletion over ca. 3.5, 1.5, and 1 h, respectively (Scheme 4). Complex **1** gave a mixture of fac-$[Ru(PPh_3)_2(C_6H_4PPh_2)H_2]$-$[Li(THF)_n]$ (**7-Li**)[40,54] and fac-$[Ru(PPh_3)_3H_3][Li(THF)_3]$ (**8-Li**),[40−43,55,56] which, over 24 h, converted completely to **8-Li**. The reaction of **2** with H_2 proceeded with dissociation of the crown ligand from Li to also yield a mixture of **7-Li** and **8-Li**, whereas **3** yielded $[Ru(PPh_3)_3H_3][MgMe(THF)_n]$ (**8-Mg**) as the major product,[57] without formation of any significant quantities of **7-Mg** (ESI).

In stark contrast, we observed 50% loss of **4** under 1 atm H_2 in only ca. 35 min even at −40 °C. The major product was identified as mer-$[Ru(PPh_3)_3H_3(ZnMe)]$ (mer-**8-Zn**, Scheme 5), along with a minor amount of what is assigned as fac-**7-Zn**.[58] Upon warming to 0 °C, mer-**8-Zn** isomerized to fac-**8-Zn** which, upon standing at room temperature, gave the Zn-bridged ruthenium dimer, fac-$[\{Ru(PPh_3)_3H_3\}_2Zn]$ (fac-**8-Zn′**; ESI).[43,59,60]

A further interesting feature of the reaction of **4** with H_2 (performed at −10 °C) was that whereas agitation resulted in a

https://dx.doi.org/10.1021/jacs.0c01062
J. Am. Chem. Soc. 2020, 142, 6340−6349

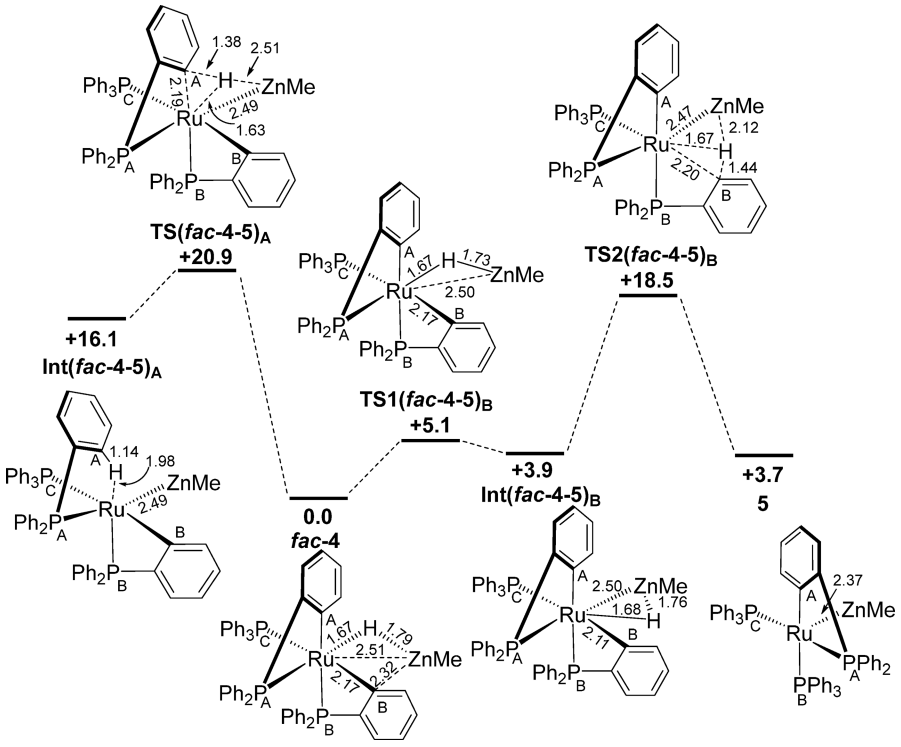

Figure 4. Computed reaction profiles (free energies, kcal/mol) for C_B–H reductive elimination and C_A–H reductive elimination pathways from *fac*-**4**. Selected distances are shown in Å.

Scheme 4. Reactivity of 1–3 with H_2

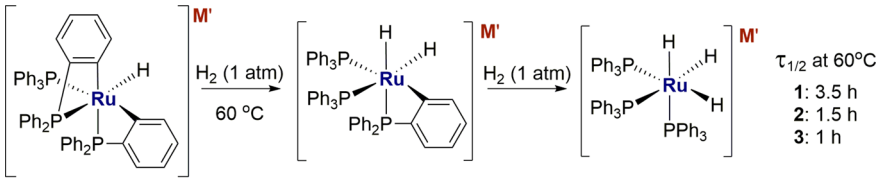

Scheme 5. Reactivity of 4 with H_2

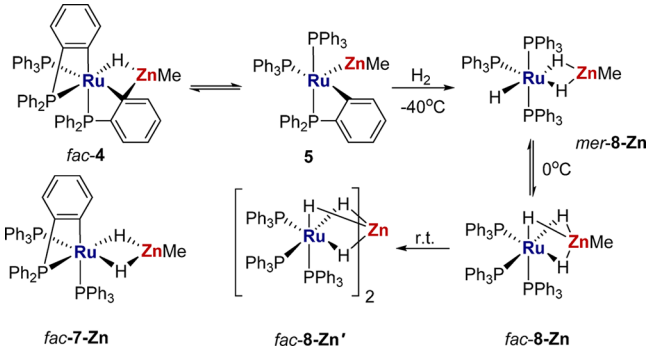

rapid change of color from red to yellow, the red color quickly reappeared when stirring was stopped. This process was repeatable several times until **4** was completely consumed (ca. 2 min of stirring see video file in the Supporting Information). This behavior can be rationalized by assuming that **5** is an intermediate in the reaction of fac-**4** with H_2 (Scheme 5) and that (as shown below) the onward reaction of **5** with H_2 is facile. Red **5** would therefore quickly react with H_2 and would only slowly accumulate in solution when H_2 is deficient due to slow diffusion (i.e., with no stirring). The mer-arrangement of phosphine ligands in **5** would also explain the exclusive formation of mer-**8-Zn** upon addition of H_2 to fac-**4** at low temperature.

The computed reaction profile for the reaction of **5** with H_2 is summarized in Scheme 6(i). Addition of H_2 to **5** is barrierless and forms a dihydrogen complex **5.H$_2$** at +5.2 kcal/mol from which C–H reductive elimination yields **Int(5-*mer*-8)** through a transition state at 14.1 kcal/mol. Both these processes occur at the unsaturated Ru center in **5**, but the dual unsaturated **Int(5-*mer*-8)** can then accommodate a further equivalent of H_2 via a barrierless reaction that proceeds with net addition of H_2 across the Ru–Zn vector to form ***mer*-8-Zn**.

To highlight the effect of Zn on these processes, we characterized the analogous profile for $[Ru(PPh_3)(PPh_2C_6H_4)_2H]^-$ (**2**) for which the initial C–H reductive elimination entails a significantly higher barrier of 24.4 kcal/mol [Scheme 6(ii)]. This leads to the 4-coordinate Ru(0) anion $[Ru(PPh_3)_2(PPh_2C_6H_4)]^-$ ($\mathbf{5_H}$) at +16.6 kcal/mol which can then undergo facile oxidative addition of H_2 to give $\mathbf{7_H}$ (−8.8 kcal/mol). C–H reductive elimination then proceeds with a barrier of 21.2 kcal/mol to form **Int(7–8)$_H$** at +7.4 kcal/mol that can then engage in a barrierless addition of a second molecule of H_2 to give $\mathbf{8_H}$. Thus, the greater reactivity of ***fac*-4** with H_2 is linked to the kinetically more accessible

https://dx.doi.org/10.1021/jacs.0c01062
J. Am. Chem. Soc. 2020, 142, 6340–6349

Scheme 6. Summaries of the Computed Profiles for C−H Reductive Elimination and the Onward Reactions with H_2 of (i) *fac*-4 and (ii) the Anion of 2[a]

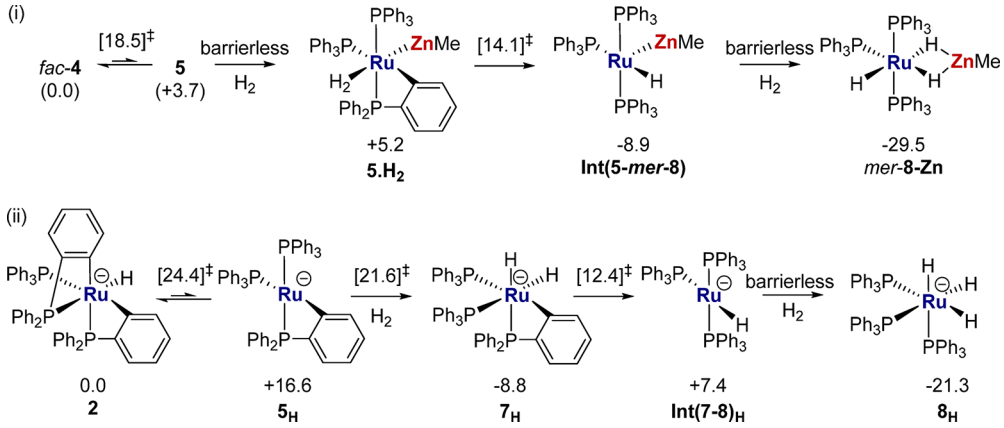

[a]Relative free energies are in kcal/mol and full details of all profiles are provided in the Supporting Information.

initial C−H reductive elimination to form **5** ($\Delta G^{\ddagger}$ = 18.5 kcal/mol) compared to that in **2** ($\Delta G^{\ddagger}$ = 24.4 kcal/mol). The resulting dual unsaturated Ru−Zn intermediate **5** (+3.7 kcal/mol) is also being significantly stabilized compared to Zn-free $\mathbf{5_H}$ (+16.6 kcal/mol), greatly favoring the pre-equilibrium population of the formally Ru(0) species in the presence of Zn.

The role of Zn in stabilizing species **5** was further probed (Figure 5).[61] A QTAIM study identifies a Ru−Zn bond path

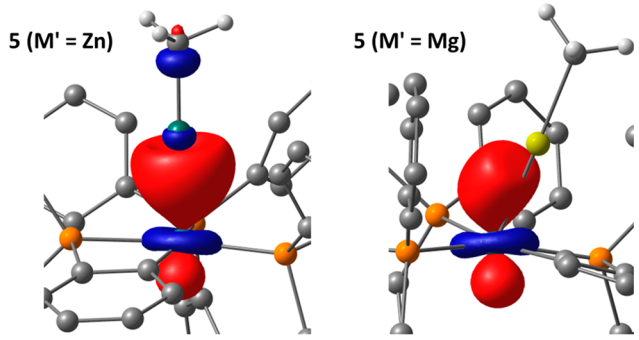

Relative Energy	+3.7 kcal/mol	+12.7 kcal/mol
Ru–M′	2.37 Å	2.52 Å
NLMO	78% (Ru), 13 % (Zn)	88% (Ru), 5 % (Mg)
$LP_{Ru} \rightarrow \sigma^*_{M'-Me}$	129 kcal/mol	30 kcal/mol
Wiberg BI	0.42	0.22
Ru-M' BCP ρ(r)	0.075 a.u.	0.037 a.u.

Figure 5. Electronic structure analysis of **5** and its Mg congener $\mathbf{5_{Mg}}$ illustrating the major NLMO contributing to Ru−M′ bonding in each case.

with a BCP $\rho(r)$ of 0.075 au, a similar value to that characterized for the $[Ru(IPr)_2(CO)(ZnEt)]^+$ cation.[62] NBO also identifies a major interaction between a Ru lone pair (equating to the $4d_z^2$ orbital) and the Zn−Me σ^* orbital, which is quantified via second-order perturbation analysis at 129 kcal/mol. The resultant NLMO shown in Figure 5 is heavily weighted toward Ru but does show a 13% Zn character. A Ru−Zn Wiberg bond index of 0.42 is computed.

To place these results in context, we have also considered the analogous Mg complex, $\mathbf{5_{Mg}}$. This is computed to lie 12.7 kcal/mol above ***fac*-4$_{Mg}$**, the analogue of the Zn reactant ***fac*-4**, signaling a lower ability of Mg to stabilize the Ru(0) metal center compared to Zn. That $\mathbf{5_{Mg}}$ is also much closer in energy to $\mathbf{5_H}$ is also consistent with the lower reactivity of the Mg system seen experimentally.[63] The computed structure of $\mathbf{5_{Mg}}$ exhibits a similar square-pyramidal structure to **5**, although with a tilting of the Ru−Mg−Me vector toward the remaining cyclometalated carbon (Mg···C = 2.52 Å). The Ru−Mg distance of 2.52 Å is 0.15 Å longer than the Ru−Zn distance in **5**. All other computed metrics point to a significantly weaker Ru···Mg interaction in $\mathbf{5_{Mg}}$: reduced Mg character in the relevant NLMO, weaker $LP_{Ru} \rightarrow \sigma^*_{Mg-Me}$ donation, and a reduced Wiberg bond index and RuMg BCP electron density.

The computed structures of the rate-limiting C−H reductive elimination transition states also highlight the role of Zn in promoting this process (see Figure 6 which also shows comparative data for the immediate precursors to C−H reductive elimination). For Zn, **TS2(*fac*-4−5)$_B$** displays a 4-centered structure with a near-linear Zn···H···C unit and a short Ru−H distance of 1.67 Å. The Ru−Zn distance shortens slightly in the transition state, and little change in the P^1−Rh−P^2 angle is computed. This structure closely resembles σ-bond metathesis transition states computed for late-transition metal centers.[64,65] In contrast, $\mathbf{TS(2-5)_H}$ is a 3-centered transition state in which C−H bond formation is far more advanced and a significant widening of P−Ru−P angle is computed. The transition state in the Mg system, **TS2(*fac*-4−5)$_{B-Mg}$**, lies between these two extremes, but unlike its Zn congener, no shortening of the Ru−Mg distance is seen.[66] The computed NBO charges (in italics, Figure 6) all indicate the transferring H to have significant protic character in the transition state. However, as the precursors in the heterobimetallic systems show significant hydride character, the degree of charge distribution is far greater for these systems. This excess charge is accommodated by the Ru−M′ moiety and appears to be facilitated in the Zn system by the greater Ru−Zn interaction.

CONCLUSIONS

Reaction of $[Ru(PPh_3)_3HCl]$ with $LiCH_2TMS$, $MgMe_2$, and $ZnMe_2$ proceeds with chloride abstraction and alkane elimination to form the bis-cyclometalated salts $[Ru(PPh_3)(C_6H_4PPh_2)_2H][M']$ ([M′] = $[Li(THF)_2]^+$ (**1**), $[MgMe(THF)_2]^+$ (**3**)) and the complex $[Ru(PPh_3)(C_6H_4PPh_2)_2H$-

https://dx.doi.org/10.1021/jacs.0c01062
J. Am. Chem. Soc. 2020, 142, 6340−6349

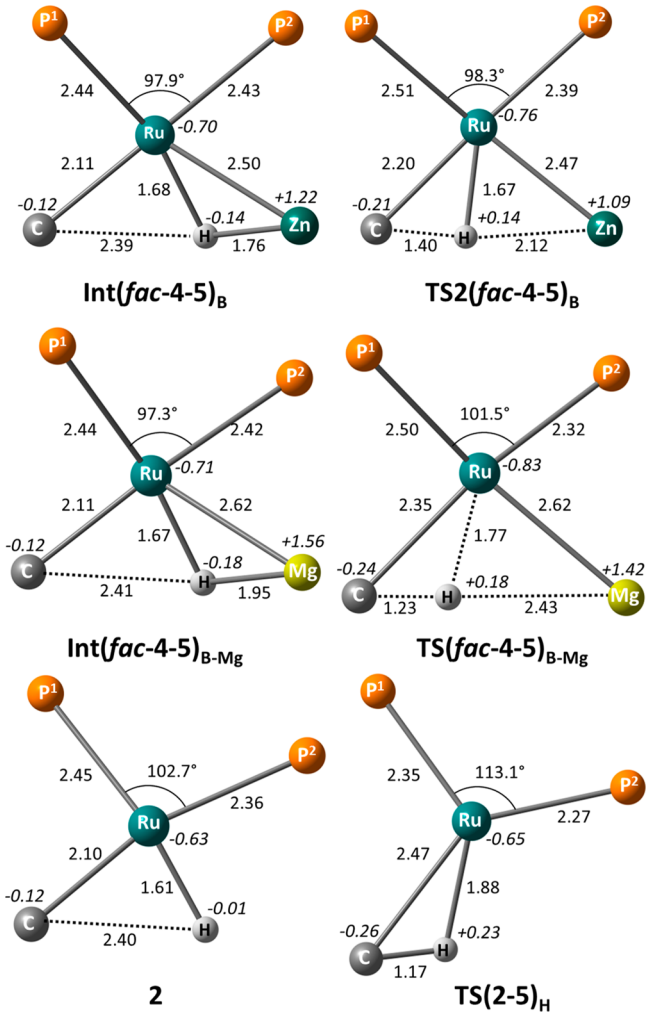

Figure 6. Computed key distances (Å) in the rate-limiting C−H reductive elimination transition states and their immediate precursors for the Zn and Mg systems and anion **2**. NBO charges are also indicated in italics.

(ZnMe)] (**4**). Upon treatment of **1** with 12-crown-4, the $[Li(12\text{-crown-}4)_2]^+$ derivative, **2**, is produced. Experimental and computational studies show increasing covalent interaction between the [M′] cations with the Ru−H ligand along the series **2** < **1** < **3** < **4**, both in the solid-state and in solution. The Zn species **4** exists as three isomers in solution: a dominant fac isomer, together with a minor mer isomer and a minor third species formulated as $[Ru(PPh_3)_2(C_6H_4PPh_2)(ZnMe)]$, **5**, which is formed via C−H reductive elimination. The DFT-computed structure of **5** features a square-pyramidal geometry with an axial ZnMe ligand and unsaturated Ru and Zn centers. **5** is computed to lie 3.7 kcal/mol above ***fac*-4**. Further support for the structure of **5** comes from the isolation and crystallographic characterization of a $[ZnMe]^+$ trapped adduct, $[Ru(PPh_3)_2(C_6H_4PPh_2)(ZnMe)_2][BAr^F{}_4]$ (**6**).

Compound **4** undergoes efficient reaction with H_2 at −40 °C to form $[Ru(PPh_3)_3H_3(ZnMe)]$, **8-Zn**. In marked contrast, the analogous reactions of **1**, **2**, and **3** all require extended heating at 60 °C. This difference is attributed to the ability of the $[ZnMe]^+$ moiety to promote C−H reductive elimination in ***fac*-4** to form **5**, a step that DFT calculations identify as the overall rate-limiting process in these hydrogenation reactions. With ***fac*-4**, a barrier to reductive elimination of 18.5 kcal/mol is computed, significantly below the value of 24.4 kcal/mol for the free $[Ru(PPh_3)(C_6H_4PPh_2)_2H]^-$ anion. QTAIM and NBO calculations show the Ru(0) metal center in **5** is significantly stabilized by donation from the Ru $4d_{z^2}$ orbital to the Z-type $[ZnMe]^+$ ligand and that this effect is significantly attenuated in the Mg analogue. ***Fac*-4** therefore acts as a latent source of **5**. This operational dual unsaturation highlights the ability of Zn to promote reductive elimination in these heterobimetallic systems. Calculations also highlight the ability of the heterobimetallic systems to stabilize developing protic character of the transferring hydrogen in the rate-limiting C−H reductive elimination transition states.

Our work also showcases how the alkane elimination strategy (coupled here with chloride abstraction) provides straightforward access to novel heterobimetallic complexes from simple organometallic precursors.[17,18,30,31] The resulting dual unsaturated systems also feature unsupported TM-main group bonds that provide a well-defined platform for detailed mechanistic studies of the heterobimetallic effect on reactivity.

The present systems, in which strong Z-type interactions[4] facilitate ligand reductive elimination represents a novel mode of activation of anionic TM complexes. These contrast previous approaches to enhance the reactivity of anionic TM complexes, which commonly rely on the use of weakly interacting counter-cations M′ ($[(2,2,2\text{-cryptand})K]^+$, etc.) in order to increase the nucleophilicity of a system.[67] Here we have demonstrated that the higher level of interaction between a TM anion and M′ cation can also be advantageous for reactivity.

■ ASSOCIATED CONTENT

Supporting Information

The Supporting Information is available free of charge at https://pubs.acs.org/doi/10.1021/jacs.0c01062.

Experimental and computational details, including characterization data (PDF)
CIF file (CIF)
Reaction of **4** while stirring (MP4)
Computed geometries (XYZ)

■ AUTHOR INFORMATION

Corresponding Authors

Fedor M. Miloserdov − *Department of Chemistry, University of Bath, Bath, U.K.*; orcid.org/0000-0001-6420-211X; Email: fm593@bath.ac.uk

Stuart A. Macgregor − *Institute of Chemical Sciences, Heriot-Watt University, Edinburgh EH14 4AS, U.K.*; orcid.org/0000-0003-3454-6776; Email: s.a.macgregor@hw.ac.uk

Michael K. Whittlesey − *Department of Chemistry, University of Bath, Bath, U.K.*; orcid.org/0000-0002-5082-3203; Email: m.k.whittlesey@bath.ac.uk

Authors

Nasir A. Rajabi − *Institute of Chemical Sciences, Heriot-Watt University, Edinburgh EH14 4AS, U.K.*; orcid.org/0000-0001-5623-797X

John P. Lowe − *Department of Chemistry, University of Bath, Bath, U.K.*; orcid.org/0000-0003-4820-251X

Mary F. Mahon − *Department of Chemistry, University of Bath, Bath, U.K.*

Complete contact information is available at: https://pubs.acs.org/10.1021/jacs.0c01062

https://dx.doi.org/10.1021/jacs.0c01062
J. Am. Chem. Soc. 2020, 142, 6340−6349

Notes

The authors declare no competing financial interest.

■ ACKNOWLEDGMENTS

We acknowledge financial support from the EU (Marie Curie Individual Fellowship to F.M.M.; 792674 H2020-MSCA-IF 2017) and Heriot-Watt University (James Watt Scholarship to N.A.R.). We dedicate this paper to Professor Pablo Espinet in belated celebration of his 70th birthday.

■ REFERENCES

(1) Hartwig, J. F. *Organotransition Metal Chemistry: From Bonding to Catalysis*; University Science Books: Sausalito, CA, 2010.
(2) Gemel, C.; Steinke, T.; Cokoja, M.; Kempter, A.; Fischer, R. A. Transition metal chemistry of low valent group 13 organyls. *Eur. J. Inorg. Chem.* **2004**, *2004*, 4161−4176.
(3) Whitmire, K. H. In *Comprehensive Organometallic Chemistry II*; Mingos, D. M. P., Crabtree, R. H., Eds.; Elsevier: Oxford, 2007; Vol. *3*, pp 343−407.
(4) Amgoune, A.; Bourissou, D. σ-Acceptor, Z-type ligands for transition metals. *Chem. Commun.* **2011**, *47*, 859−871.
(5) Bauer, J.; Braunschweig, H.; Dewhurst, R. D. Metal-only Lewis pairs with transition metal Lewis bases. *Chem. Rev.* **2012**, *112*, 4329−4346.
(6) *Molecular Metal-Metal Bonds: Compounds, Synthesis, Properties*; Liddle, S. T., Ed.; Wiley-VCH: Weinheim, Germany, 2015.
(7) Maity, A.; Teets, T. S. Main group Lewis acid-mediated transformations of transition metal hydride complexes. *Chem. Rev.* **2016**, *116*, 8873−8911.
(8) Butler, M. J.; Crimmin, M. R. Magnesium, zinc, aliminium and gallium hydride complexes of the transition metals. *Chem. Commun.* **2017**, *53*, 1348−1365.
(9) Liberman-Martin, A. L.; Levine, D. S.; Ziegler, M. S.; Bergman, R. G.; Tilley, T. D. Lewis acid-base interactions between platinium(II) diaryl complexes and bis(perfluorophenyl)zinc: Strongly accelerated reductive elimination induced by a Z-type ligand. *Chem. Commun.* **2016**, *52*, 7039−7042.
(10) Cammarota, R. C.; Lu, C. C. Tuning nickel with Lewis acidic group 13 metalloligands for catalyic olefin hydrogenation. *J. Am. Chem. Soc.* **2015**, *137*, 12486−12489.
(11) Cammarota, R. C.; Vollmer, M. V.; Xie, J.; Ye, J. Y.; Linehan, J. C.; Burgess, S. K.; Appel, A. M.; Gagliardi, L.; Lu, C. C. A bimetallic nickel-gallium complex catalyzes CO_2 hydrogenation via the intermediacy of an anionic d^{10} nickel hydride. *J. Am. Chem. Soc.* **2017**, *139*, 14244−14250.
(12) Cammarota, R. C.; Clouston, L. J.; Lu, C. C. Leveraging molecular metal-support interactions for H_2 and N_2 activation. *Coord. Chem. Rev.* **2017**, *334*, 100−111.
(13) Derrah, E. J.; Sircoglou, M.; Mercy, M.; Ladeira, S.; Bhouhadir, G.; Miqueu, K.; Maron, L.; Bourissou, D. Original transition metal→ indium interactions upon coordination of a triphosphine-indane. *Organometallics* **2011**, *30*, 657−660.
(14) Takaya, J.; Iwasawa, N. Palladium complexes bearing a group 13 metalloligand: Remarkable effect of an aluminium-metalloligand in hydrosilylation of CO_2. *J. Am. Chem. Soc.* **2017**, *139*, 6074−6077.
(15) Steinhoff, P.; Paul, M.; Schroers, J. P.; Tauchert, M. E. Highly efficient palladium-catalysed carbon dioxide hydrosilylation employing PMP ligands. *Dalton Trans.* **2019**, *48*, 1017−1022.
(16) IPr = 1,3-bis(2,6-diisopropylphenyl)imidazol-2-ylidene.
(17) Riddlestone, I. M.; Rajabi, N. A.; Lowe, J. P.; Mahon, M. F.; Macgregor, S. A.; Whittlesey, M. K. Activation of H_2 over the Ru-Zn bond in the transition metal-Lewis acid heterobimetallic species $[Ru(IPr)_2(CO)ZnEt]^+$. *J. Am. Chem. Soc.* **2016**, *138*, 11081−11084.
(18) Riddlestone, I. M.; Rajabi, N. A.; Macgregor, S. A.; Mahon, M. F.; Whittlesey, M. K. Well-defined heterobimetallic reactivity at unsupported ruthenium-indium bonds. *Chem. - Eur. J.* **2018**, *24*, 1732−1738.
(19) Tebbe, F. N. Lewis acidic metal alkyl-transition metal complex interactions. I. Niobium and tantalum hydrides. *J. Am. Chem. Soc.* **1973**, *95*, 5412−5414.
(20) St. Denis, J. N.; Butler, W.; Glick, M. D.; Oliver, J. P. Studies on main group metal-transition metal bonded compounds. II. The crystal and molecular structure of π-$C_5H_5(CO)_3WGa(CH_3)_2$ and evidence for mixed organozinc and organogallium transition metal derivatives. *J. Organomet. Chem.* **1977**, *129*, 1−16.
(21) Budzelaar, P. H. M.; Den Haan, K. H.; Boersma, J.; van der Kerk, G. J. M.; Spek, A. L. Reaction of $(C_5H_5)_2NbH_3$ with $(C_5H_5)_2Zn$ - structure of $(C_5H_5)_2NbH_2ZnC_5H_5$. *Organometallics* **1984**, *3*, 156−159.
(22) Bruno, J. W.; Huffman, J. C.; Caulton, K. G. Aluminium alkyls and transition metal hydrides: ″Nonclassical″ adduct structure and catalysis of hydrogen migration. *J. Am. Chem. Soc.* **1984**, *106*, 444−445.
(23) Thorn, D. L.; Harlow, R. L. Transition metal-organo-indium chemistry. Addition of alkyl-indium bonds to alkyliridium complexes and the structure of $IrH(Et)(Et_2In)(PMe_3)_3$. *J. Am. Chem. Soc.* **1989**, *111*, 2575−2580.
(24) Fryzuk, M. D.; McConville, D. H.; Rettig, S. J. Fragmentation-recombination reactions of the electron-rich binuclear hydride $[\{Pr^i_2PCH_2CH_2CH_2PPr^i_2\}Rh]_2(\mu\text{-}H)_2$ with dibenzylzinc. X-ray structure of $[\{Pr^i_2PCH_2CH_2CH_2PPr^i_2\}Rh]_2(\mu\text{-}H)_2(\mu\text{-}ZnCH_2Ph)_2$. *Organometallics* **1990**, *9*, 1359−1360.
(25) Fryzuk, M. D.; McConville, D. H.; Rettig, S. J. Reactions of the electron-rich binuclear hydride complexes $[\{Pr^i_2P(CH_2)_xPPr^i_2\}Rh]_2(\mu\text{-}H)_2$ (x = 2 or 3) with ZnR_2 and MgR'_2. *Organometallics* **1993**, *12*, 2152−2161.
(26) Golden, J. T.; Peterson, T. H.; Holland, P. L.; Bergman, R. G.; Andersen, R. A. Adduct formation and single and double deprotonations of $Cp^*(PMe_3)Ir(H)_2$ with main group metal alkyls and aryls: Synthesis and structure of three novel Ir-Al and Ir-Mg heterobimetallics. *J. Am. Chem. Soc.* **1998**, *120*, 223−224.
(27) Ohashi, M.; Matsubara, K.; Suzuki, H. Ruthenium polyhydrido clusters having a bridging alkylzinc group, $[(\eta^5\text{-}C_5Me_5)Ru(\mu\text{-}H)]_3(\mu_3\text{-}ZnR)_n(\mu_3\text{-}H)_{2-n}$ and $[(\eta^5\text{-}C_5Me_5)Ru]_2(\mu\text{-}ZnR)_n(\mu\text{-}H)_{4-n}$ (R = Me and Et; n = 1 and 2). *Organometallics* **2007**, *26*, 2330−2339.
(28) Durango-García, C. J.; Jiménez-Halla, J. O. C.; López-Cardoso, M.; Montiel-Palma, V.; Muñoz-Hernández, M. A.; Merino, G. On the nature of the transition metal-main group metal bond: Synthesis and theoretical calculations on iridium gallyl complexes. *Dalton Trans.* **2010**, *39*, 10588−10589.
(29) IMes = 1,3-bis(2,4,6-trimethylphenyl)imidazol-2-ylidene.
(30) Espinal-Viguri, M.; Varela-Izquierdo, V.; Miloserdov, F. M.; Riddlestone, I. M.; Mahon, M. F.; Whittlesey, M. K. Heterobimetallic ruthenium-zinc complexes with bulky N-heterocyclic carbenes: syntheses, structures and reactivity. *Dalton Trans.* **2019**, *48*, 4176−4189.
(31) O'Leary, N.; Miloserdov, F. M.; Mahon, M. F.; Whittlesey, M. K. Transforming PPh_3 into bidentate phosphine ligands at Ru-Zn heterobimetallic complexes. *Dalton Trans.* **2019**, *48*, 14000−14009.
(32) Cole-Hamilton, D. J.; Wilkinson, G. ortho-Metallated triphenylphosphine(2-diphenylphosphinophenyl) and related complexes of ruthenium(II): Interaction of chlorohydridotris-(triphenylphosphine)ruthenium(II) with methyl and trimethylsilylmethyl alkylating agents (Li, Mg, Zn); hydrido methyl and trimethylsilylmethyl complexes. *J. Chem. Soc., Dalton Trans.* **1977**, 797−804.
(33) The presence of two-cyclometalated phosphines at a single transition metal center remains uncommon, especially for group 8 metals. See, for example: Clark, G. R.; Lu, G.-L.; Rickard, C. E. F.; Roper, W. R.; Wright, L. J. Metallacyclic complexes with ortho-silylated triphenylphosphine ligands, $L_nOs(\kappa^2(Si,P)\text{-}SiMe_2C_6H_4PPh_2)$, derived from thermal reactions of the coordinatively unsaturated trimethylsilyl, methyl complex, $Os(SiMe_3)(Me)(CO)(PPh_3)_2$. *J. Organomet. Chem.* **2005**, *690*, 3309−3320.
(34) Bennett, M. A.; Bhargava, S. K.; Ke, M.; Willis, A. C. Complexes of platinum(II), platinum(IV), rhodium(III) and iridium-

https://dx.doi.org/10.1021/jacs.0c01062
J. Am. Chem. Soc. 2020, 142, 6340−6349

(III) containing orthometallated triphenylphosphine. *J. Chem. Soc., Dalton Trans.* **2000**, 3537−3545.
(35) Mohr, F.; Privér, S. H.; Bhargava, S. K.; Bennett, M. A. Ortho-metalated transition metal complexes derived from tertiary phosphine and arsine ligands. *Coord. Chem. Rev.* **2006**, *250*, 1851−1888.
(36) Bennett, M. A.; Bhargava, S. K.; Messelhäuser, J.; Privér, S. H.; Welling, L. L.; Willis, A. C. ortho-Metallated complexes of platinum(II) and diplatinum(I) containing the carbanions (2-diphenylphosphino)phenyl and (2-diphenylphosphino)-n-tolyl (n = 5, 6). *Dalton Trans.* **2007**, 3158−3169.
(37) Garrou, P. E. Δ_R ring contributions to ^{31}P NMR parameters of transition-metal-phosphorus chelate complexes. *Chem. Rev.* **1981**, *81*, 229−266.
(38) Millard, M. D.; Moore, C. E.; Rheingold, A. L.; Figueroa, J. S. Four-coordinate iridium(I) monohydrides: Reversible dinitrogen binding, bond activations and deprotonations. *J. Am. Chem. Soc.* **2010**, *132*, 8921−8923.
(39) del Pozo, J.; Pérez-Iglesias, M.; Álvarez, R.; Lledós, A.; Casares, J. A.; Espinet, P. Speciation of $ZnMe_2$, ZnMeCl, and $ZnCl_2$ in tetrahydrofuran (THF), and its influence on mechanism calculations of catalytic processes. *ACS Catal.* **2017**, *7*, 3575−3583.
(40) Pez, G. P.; Grey, R. A.; Corsi, J. Anionic metal hydride catalysts. 1. Synthesis of potassium hydrido(phosphine)ruthenate complexes. *J. Am. Chem. Soc.* **1981**, *103*, 7528−7535.
(41) Chan, A. S. C.; Shieh, H.-S. New synthesis and molecular structure of potassium trihydrido(triphenylphosphine)ruthenate. *J. Chem. Soc., Chem. Commun.* **1985**, 1379−1380.
(42) Plois, M.; Hujo, W.; Grimme, S.; Schwickert, C.; Bill, E.; de Bruin, B.; Pöttgen, R.; Wolf, R. Open-shell first-row transition-metal polyhydride complexes based on the fac-$[RuH_3(PR_3)_3]^-$ building block. *Angew. Chem., Int. Ed.* **2013**, *52*, 1314−1318.
(43) Plois, M.; Wolf, R.; Hujo, W.; Grimme, S. Towards reagents for bimetallic activation reactions: Polyhydride complexes with Ru_2H_3, Ru_2ZnH_6, and $Cu_2Ru_2H_6$ cores. *Eur. J. Inorg. Chem.* **2013**, *2013*, 3039−3048.
(44) Cordero, B.; Gómez, V.; Platero-Prats, A. E.; Revés, M.; Echeverría, J.; Cremades, E.; Barragán, F.; Alvarez, S. Covalent radii revisited. *Dalton Trans.* **2008**, 2832−2838.
(45) Markies, P. R.; Schat, G.; Akkerman, O. S.; Bickelhaupt, F.; Smeets, W. J. J.; Spek, A. L. Coordinational behavior of solvent-free diorganylzinc compounds: The remarkable X-ray structure of dimeric diphenylzinc. *Organometallics* **1990**, *9*, 2243−2247.
(46) For comparison, trans-$^2J_{HP}$ is ca. 81 Hz in the potassium salt of $[Ru(PPh_3)_2(C_6H_4PPh_2)H]^-$. See ref 40.
(47) The level of interaction between Li and the hydride ligand in **1** was probed by ^{7}Li NMR spectroscopy and found to be solvent-dependent. While no $^1J_{Li-H}$ coupling was observed in THF-d_8, a $^1J_{Li-H}$ splitting of 12 Hz was seen in C_6D_6.
(48) Kumar, A.; Beattie, N. A.; Pike, S. D.; Macgregor, S. A.; Weller, A. S. The simplest amino-borane $H_2B{=}NH_2$ trapped on a rhodium dimer: Pre-catalysts for amine-borane dehydrogenation. *Angew. Chem., Int. Ed.* **2016**, *55*, 6651−6656.
(49) This was confirmed by an NBO study in which second-order perturbation theory identified $\sigma_{Ru-H} \rightarrow \sigma^*_{Zn-C}$ donation to be dominant and ca. 3 times greater than $\sigma_{Ru-C(B)} \rightarrow \sigma^*_{Zn-C}$ donation and 30 times greater than any $LP_{Ru} \rightarrow \sigma^*_{Zn-C}$ donation. See the Supporting Information for details, along with a noncovalent interaction plot for **4**.
(50) A detailed discussion of the structure and bonding in **6** will be the subject of a future manuscript.
(51) Exchange cross-peaks between P_{B1} and P_{C1} in fac-**4** were the only other signals that were detected. This exchange process evidently occurs via C_B-H bond formation.
(52) Häller, L. J. L.; Page, M. J.; Erhardt, S.; Macgregor, S. A.; Mahon, M. F.; Naser, M. A.; Vélez, A.; Whittlesey, M. K. Experimental and computational investigation of C-N bond activation in ruthenium N-heterocyclic carbene complexes. *J. Am. Chem. Soc.* **2010**, *132*, 18408−18416.
(53) Pell, C. J.; Shih, W. C.; Gatard, S.; Ozerov, O. V. Formation of (PNP)Rh complexes containing covalent rhodium-zinc bonds in studies of potential Rh-catalysed Negishi coupling. *Chem. Commun.* **2017**, *53*, 6456−6459.
(54) Grey, R. A.; Pez, G. P.; Wallo, A.; Corsi, J. Homogeneous catalytic hydrogenation of carboxylic acid esters to alcohols. *J. Chem. Soc., Chem. Commun.* **1980**, 783−784.
(55) Wilczynski, R.; Fordyce, W. A.; Halpern, J. Coordination chemistry and catalytic properties of hydrido(phosphine)ruthenate complexes. *J. Am. Chem. Soc.* **1983**, *105*, 2066−2068.
(56) Fordyce, W. A.; Wilczynski, R.; Halpern, J. Hydrido-(phosphine)ruthenate complexes and their role in the catalytic hydrogenation of arenes. *J. Organomet. Chem.* **1985**, *296*, 115−125.
(57) For examples of Ru-H-M′ (M′ = Zn, Mg) species, see: Lau, S.; White, A. J. P.; Casely, I. J.; Crimmin, M. R. Tunable binding of dinitrogen to a series of heterobimetallic hydride complexes. *Organometallics* **2018**, *37*, 4521−4526.
(58) This was shown to form as a side-product in the reaction rather than an intermediate on the way to mer-**8**-Zn. See the Supporting Information.
(59) Interestingly, mer-**4** was found to be much less reactive than fac-**4** toward H_2, since the diagnostic hydride signal of the former could still be observed even at room temperature after all of the fac-**4** had reacted at −40 °C. The computed barrier for C-H reductive elimination from mer-**4** is 21.8 kcal/mol, 3.3 kcal/mol above that for fac-**4**.
(60) For a related Ru-H-Zn bonding situation, see: Molon, M.; Gemel, C.; Fischer, R. From AlCp*- and GaCp*-ligated ruthenium hydrides to zinc-rich heterometallic complexes. *Eur. J. Inorg. Chem.* **2013**, *2013*, 3616−3622.
(61) Paenurk, E.; Gershoni-Poranne, R.; Chen, P. Trends in metallophilic bonding in Pd-Zn and Pd-Cu complexes. *Organometallics* **2017**, *36*, 4854−4863.
(62) Rajabi, N. A. DFT studies on heterobimetallic complexes of Ru with Zn, Ga and In. Ph.D. Thesis, Heriot-Watt University, 2018.
(63) We also considered the effect of maintaining THF bound to Mg on the free energy change of reductive elimination. With one THF, ΔG is computed to be +12.2 kcal/mol; for two THF, ΔG = 21.0 kcal/mol. See the Supporting Information for full details.
(64) Boutadla, Y.; Davies, D. L.; Macgregor, S. A.; Poblador-Bahamonde, A. I. Mechanisms of C-H bond activation: Rich synergy between computation and experiment. *Dalton Trans.* **2009**, 5820−5831.
(65) Balcells, D.; Clot, E.; Eisenstein, O. C-H Bond activation in transition metal species from a computational perspective. *Chem. Rev.* **2010**, *110*, 749−823.
(66) An overall barrier of 28.8 kcal/mol was computed for the Mg system which used a model without any THF molecules bound to Mg in order to aid comparison with the Zn congener. Test calculations on $\mathbf{5_{Mg}}$ indicate that including one or two THF does destabilize this species (see ref 63). However, the speciation of this Mg system during the reaction is unclear, and this may lie behind the anomalously high computed barrier. On the other hand, the computed barrier for the reductive elimination step is smaller for Mg (i.e., $\mathbf{Int}(\mathit{fac}\text{-}\mathbf{4}{-}\mathbf{5})_{\mathbf{B\text{-}Mg}}$ to $\mathbf{TS}(\mathit{fac}\text{-}\mathbf{4}{-}\mathbf{5})_{\mathbf{B}}$ = 22.4 kcal/mol) than for the free anion (**2** to $\mathbf{TS}(\mathbf{2}{-}\mathbf{5})_{\mathbf{H}}$ = 24.4 kcal/mol), and this does suggest a stabilizing effect of Mg, and one that is substantially less than for Zn ($\mathbf{Int}(\mathit{fac}\text{-}\mathbf{4}{-}\mathbf{5})_{\mathbf{B}}$ to $\mathbf{TS}(\mathit{fac}\text{-}\mathbf{4}{-}\mathbf{5})_{\mathbf{B}}$ = 14.6 kcal/mol).
(67) Gómez-Suárez, A.; Nelson, D. J.; Nolan, S. P. Metallate complexes of the late transition metals: organometallic chemistry and catalysis. *Adv. Organomet. Chem.* **2018**, *69*, 283−327.

https://dx.doi.org/10.1021/jacs.0c01062
J. Am. Chem. Soc. 2020, 142, 6340−6349